PNAS RESEARCH ARTICLE | ECOLOGY

Stabilizing microbial communities by looped mass transfer

Shuang Li[a], Nafi'u Abdulkadir[a], Florian Schattenberg[a], Ulisses Nunes da Rocha[a], Volker Grimm[b,c], Susann Müller[a,1], and Zishu Liu[d]

Edited by Simon Levin, Princeton University, Princeton, NJ; received October 7, 2021; accepted March 11, 2022

Building and changing a microbiome at will and maintaining it over hundreds of generations has so far proven challenging. Despite best efforts, complex microbiomes appear to be susceptible to large stochastic fluctuations. Current capabilities to assemble and control stable complex microbiomes are limited. Here, we propose a looped mass transfer design that stabilizes microbiomes over long periods of time. Five local microbiomes were continuously grown in parallel for over 114 generations and connected by a loop to a regional pool. Mass transfer rates were altered and microbiome dynamics were monitored using quantitative high-throughput flow cytometry and taxonomic sequencing of whole communities and sorted subcommunities. Increased mass transfer rates reduced local and temporal variation in microbiome assembly, did not affect functions, and overcame stochasticity, with all microbiomes exhibiting high constancy and increasing resistance. Mass transfer synchronized the structures of the five local microbiomes and nestedness of certain cell types was eminent. Mass transfer increased cell number and thus decreased net growth rates μ'. Subsets of cells that did not show net growth $\mu' SC_x$ were rescued by the regional pool R and thus remained part of the microbiome. The loop in mass transfer ensured the survival of cells that would otherwise go extinct, even if they did not grow in all local microbiomes or grew more slowly than the actual dilution rate D would allow. The rescue effect, known from metacommunity theory, was the main stabilizing mechanism leading to synchrony and survival of subcommunities, despite differences in cell physiological properties, including growth rates.

microbial ecology | metacommunity assembly | stability | microbial community cytometry | single-cell analytics

Significance

The population ecology of microbial communities is still poorly understood and their notorious instability makes them impossible to control. Much of the instability is caused by the stochastic assembly of microorganisms, especially in highly diverse microbiomes where structural and hence functional changes occur rapidly due to the short generation time of their members. Usually, to maintain organismic proportions in communities, their niches are deterministically reinforced, but stochasticity strongly counteracts this. Based on metacommunity theory, a looped mass transfer was developed that uses the rescue effect to stabilize communities. This study fills a long-standing gap and enables continuous and proportionally equal growth of community members using an unprecedented operational design that addresses an acute need in the healthcare and biotechnology industries.

The ability to create structurally and functionally stable microbiomes would be greatly beneficial to both industrial biotechnology and human health. Stable microbiomes would be persistent in their composition and hence their functions and services (1–3). Building and changing a microbiome as desired and maintaining it over hundreds of generations is a challenging endeavor that still needs to be undertaken. Stable microbiomes would make it much easier to use renewable and less-expensive resources and develop bio-based technologies as part of a circular bio-economy (4, 5). Bottom-up and top-down approaches that are based on design–build–test–learn cycles (6) to optimize artificial microbiome blueprints are promising potential avenues for the construction of human-life-promoting microbiomes (7). However, the current means of controlling microbiomes are still limited. For decades, scientists have attempted to homogenize (8) or establish stable natural and artificial communities by shaping their niches, e.g. via substrate type and concentration, media composition or pH, and temperature, including using machine learning and other mathematically based approaches (9–12). Despite all these efforts, however, complex microbiomes appear to remain susceptible to large stochastic variations.

To establish stable microbiomes, a first challenge is to quantify community composition and its change. Liu et al. (9) combined quantitative single-cell and taxonomic analyses to characterize microbial communities that comprised hundreds of species. However, when applying their approach to five parallel identically operated steady-state reactors that began from the same inoculum, they found that the five communities developed along different trajectories, leading to distinctly different compositions. One primary reason for this, as suggested by Liu et al. (9), was the ongoing disturbance in each reactor via dilution. Dilution reduced the abundance of otherwise dominant species and caused the extinction of species with low growth rates, thereby significantly increasing the role of stochasticity. Functional redundancy supported this process. Zhou et al. (13) also found 14 distinctly different communities that developed from the same inoculum, referred to as "stochastic assembly."

The important role of stochasticity in understanding community assembly has been widely acknowledged in ecology (14, 15). In particular, the work of Zhou and Ning (16), which combined the framework (i.e., diversification, dispersal, selection, and drift) of Vellend (17) and Nemergut et al. (18) with the βNTI- and βNRI-based

Author contributions: S.M. and Z.L. designed research; S.L. and S.M. performed research; S.L., N.A., F.S., U.N.d.R., and Z.L. analyzed data; S.L., V.G., and S.M. wrote the paper; and F.S., U.N.d.R., and Z.L. revised the manuscript.

The authors declare no competing interest.

This article is a PNAS Direct Submission.

[1]To whom correspondence may be addressed. Email: susann.mueller@ufz.de.

This article contains supporting information online at http://www.pnas.org/lookup/suppl/doi:10.1073/pnas.2117814119/-/DCSupplemental.

Published April 21, 2022.

approaches to assembly processes (19, 20) is now widely used to determine stochastic processes of microbial community assembly (21–24). Rank-abundance data of virtually all known communities show that, except for a few dominant species, most species occur at low abundances (25–29) and thus are strongly affected by stochasticity.

How, then, do the more or less stable communities develop which can be observed in macroecology? An answer can be found in metapopulation theory (30), which is also incorporated in metacommunity theory (31, 32). In metapopulations, small local populations (1) may go extinct but be replaced by recolonization or (2) may be "rescued" from extinction by immigration. In metacommunity theory, the former mechanism is referred to as "patch dynamics" (33). The latter is referred to as "mass effect/transfer" (34) or "rescue effect" (35). In both cases, the regional pool that comprised all local populations buffers and thereby stabilizes local populations.

A second challenge in stabilizing microbial communities is how we can mimic the stabilizing effect of the regional pool. The patch dynamics mechanism requires limited dispersal to avoid the possibility that local dynamics are overly synchronized and their disparity is kept exclusive. In contrast, the rescue effect requires more substantial dispersal from the regional pool and supports the survival of local populations that would otherwise have too low an abundance and thus be at high risk of extinction. Therefore, we hypothesize that mass transfer from a regional pool could be a means to stabilize both structural and functional properties of microbial communities. Mass transfer is a well-known phenomenon that occurs in the intestinal system (36) and in wastewater treatment plants (26, 37). Finding a simple but efficient way to implement mass transfer from a regional pool could thus be a promising avenue for understanding and building stable microbial communities with specific desired functions.

Based on the setup that was used by Liu et al. (9), we implemented a regional pool that was connected to five parallel local communities via a loop design. Inflow from the local reactors represents emigration to the regional pool, and feedback flow represents mass transfer from the regional pool to each local community. This metacommunity that comprised six continuously running and interconnected bioreactors was established and studied for ∼114 generations with varying mass transfer rates. To quantify community dynamics, flow cytometry was used as the major methodology, which quantitatively measured community structure at the single-cell level. Additionally, selected 16S ribosomal RNA (rRNA) gene amplicon sequencing was performed for whole communities and after the directed sorting of subcommunities. We hypothesize that 1) diversity values will become more equal with higher rates of mass transfer, 2) an increase in mass transfer will strengthen the presence of slow growing organisms, and 3) high mass transfer rates will not affect function and increase the stability properties of constancy, resistance, and recovery (3). Answering these questions will shed light on whether looped mass transfer is a means of stabilizing microbial communities over extended periods of time and what ecological mechanisms are responsible for this stabilization.

Results

Mass Transfer Stabilizes Structures and Functions of Microbiomes. In this study, we investigated whether looped mass transfer can stabilize microbial community structure and function by relying on the rescue effect. To this end, flow cytometric single-cell data, clustered into gates (G) according to phenotypic cell characteristics and considered as subcommunities (SC) were analyzed at different recycling rates (*RC*) under continuous cultivation conditions. In a first step, the structural stability properties constancy, resistance (RS), and recovery (RV) as well as functional stability by analyzing the removal efficiency of carbon, ammonium-nitrogen, and phosphorus were determined.

Two hierarchical scales (i.e., local and regional scale) were designed. For the local scale, independently inoculated and connected microbiomes were cultivated in five identically operated local reactors (i.e., local communities L1–L5; *SI Appendix*, section S1). For the regional scale, a pool R of emigrated microorganisms from L1–L5 was formed from which dispersion back into the local scale was allowed (Fig. 1 and *SI Appendix*, section S2). We followed this setup for ∼114 generations, and a total of 448 community samples (with a total of 35,840 subcommunities [SC]) were collected from the six bioreactors (*SI Appendix*, section S3). Quantitative variations in the microbiomes were analyzed at the single-cell level using flow cytometry (*SI Appendix*, sections S4 and S5) and relative variations were analyzed by 16S rRNA gene sequencing (*SI Appendix*, section S6). With this setup, we sought to determine whether changes in recycling rates *RC* (*SI Appendix*, Table S2.1) may be a means to stabilize microbiomes.

The experiment was divided into five phases, in which increasing recycling rates *RC* between the regional pool R and local reactors were tested in phases 2 to 4, whereas no exchange was allowed in phases 1 and 5. Phase 1 (Insular I) showed large variations in microbiome structures between local communities in L1–L5 despite an identical inoculum. These variations were sequentially reduced when recycling rates *RC* were increased from 10 to 80% (Fig. 2*A*). Additionally, temporal variation within each reactor decreased with an increase in *RC* (Fig. 2*B*). Fluctuations reappeared after recycling was terminated (phase 5, Insular II; Fig. 2*A*). An overview on the experiment is provided in Movie S1.

The stability properties of constancy, resistance RS, and recovery RV (2), calculated for all microbiomes L1–L5 and R, supported these findings. The five local microbiomes established the highest constancy at the highest recycling rates *RC* (*SI Appendix*, Fig. S7.1*A* and Table S7.1). The values for resistance RS were lowest between the Insular I to RC_{10} phases (mean = 0.46 ± 0.05 for L1–L5), suggesting considerable variations in local microbiomes under these conditions. During transitions from RC_{10} to RC_{50} and from RC_{50} to RC_{80}, the highest resistance RS values (mean = 0.57 ± 0.03 and 0.60 ± 0.03, respectively, for L1–L5) were found and thus represented the most stable conditions (*SI Appendix*, Fig. S7.1*B*). The values for recovery RV were low in all phases and for all microbiomes (*SI Appendix*, Table S7.2), indicating that the communities did not return to compositions of previous phases.

In addition, we tested whether increasing mass transfer rates affect the function of the six wastewater communities individually or the function of the metacommunity as a whole. Wastewater communities have the function of removing carbon, nitrogen, and phosphorus from the wastewater. Carbon is taken up into biomass or degraded to CO_2. Ammonium-nitrogen comes from biomass destruction (especially proteins: amino acids) and is removed mainly by nitrification and denitrification. Phosphorus is released into wastewater under anaerobic conditions and by cell destruction and can be removed by biomass production and accumulation as polyphosphates in biomass under mainly aerobic conditions. The analyzed data and calculation framework are provided in *SI Appendix*, section S3

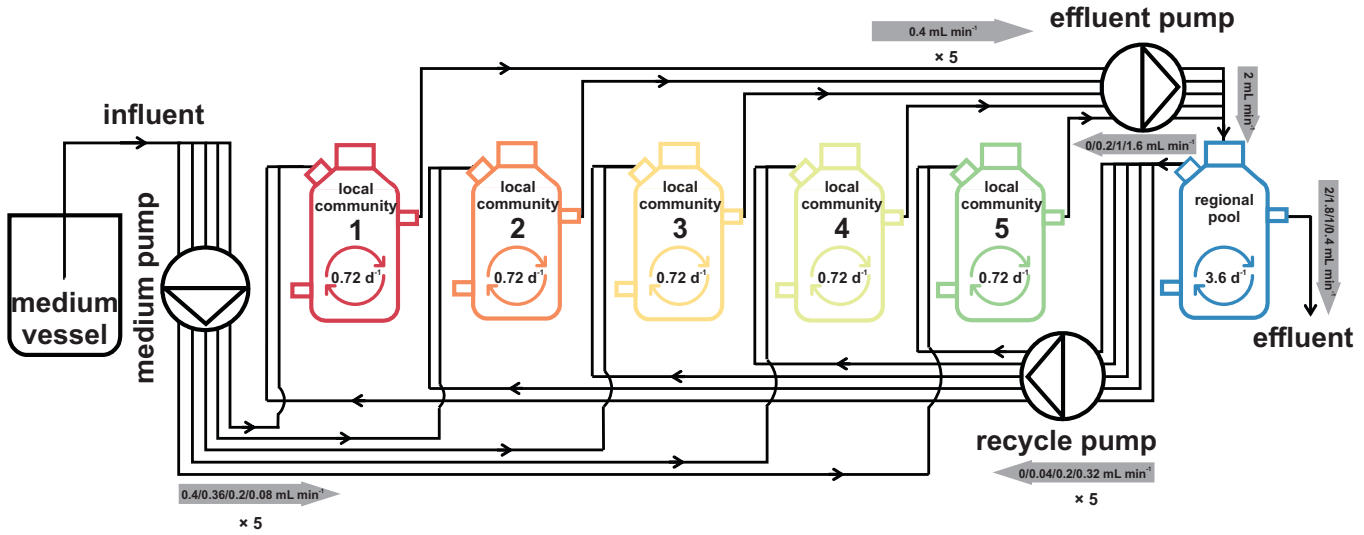

Fig. 1. Scheme of the reactor setup. The six reactors were run under the same environmental conditions. The five local community reactors L1–L5 were run in an identical mode. The sixth reactor served as the regional pool R and was fed by the effluents of the local communities L1–L5. The dilution rate per reactor is shown within the reactor schemes. A medium pump controlled the medium flow rate from the medium vessel to local communities L1–L5. An effluent pump controlled the effluent rate from the local communities to the regional pool R. A recycle pump controlled the recycling flow rate from the regional pool R to the local communities L1–L5. The flow rates are labeled with a gray arrow that indicates the flow direction.

and Tables S3.1–S3.4). Per reactor, the removal efficiency of total phosphate (PHOt) and ammonium-nitrogen in supernatant (NH4) remained about the same with increased mass transfer rates, while the removal efficiency for chemical oxygen demand of the supernatant (CODs) decreased, but only slightly. Instead, biomass (CN: cell number; CODb: carbon bound in biomass, DW: dry weight) increased with mass transfer rates. The entire metacommunity even showed increased removal efficiencies due to repeated recycling of carbon and ammonium-nitrogen in the flow (CODs: from 76.1% in RC_{10} to 87.5% in RC_{80}; NH4: 62.7% in RC_{10} to 98.5% in RC_{80}), while PHOt values remained unchanged (11.3 ± 3.2%), confirming the stable functions in the metacommunity setup with increasing mass transfer rates. Partial Mantel test revealed that the flow-cytometrically measured community composition, which changed with increasing mass transfer rates, did not influence community function in our metacommunity setup (*SI Appendix*, section S13).

In summary, the data suggest that high mass transfer rates clearly lowered local and temporal variations in community composition and supported such stabilizing properties as high constancy and increasing resistance of all microbiomes, whereas recovery efforts to reinstate a previous microbiome remained unimportant. In addition, the typical functions of wastewater

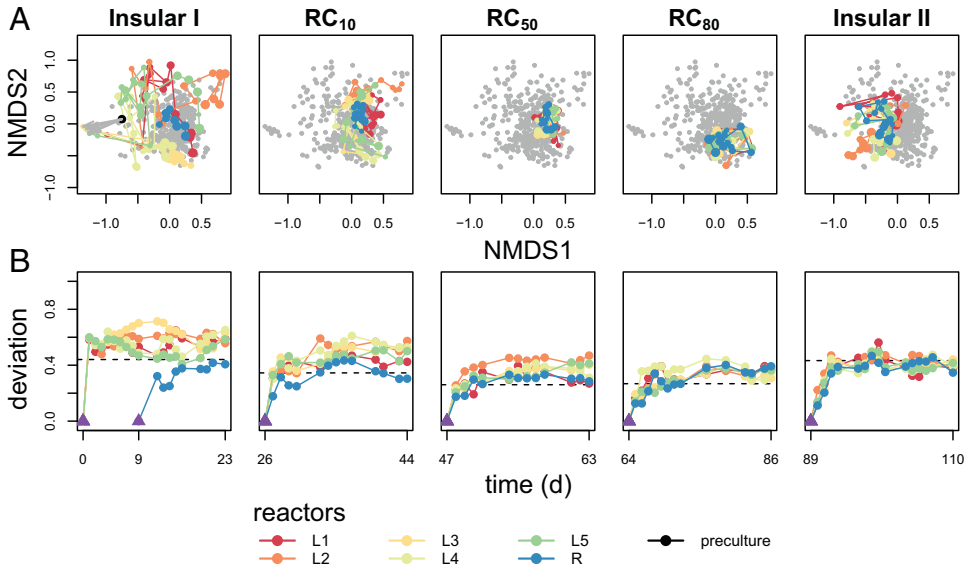

Fig. 2. Microbiome dynamics in the five reactors L1–L5 and regional pool R. Microbiome dynamics were measured by flow cytometry. The plots represent the five different phases of the experiment. In phase 1 (Insular I), L1–L5 were isolated. In phases 2 to 4, the recycling flow rate from reactor R increased sequentially from 10 to 80% (RC_{10} to RC_{80}). Phase 5 (Insular II) was again without recycling. (*A*) The nonmetric multidimensional scaling (NMDS) plots in the upper row show the increasing similarity of communities, both within and between reactors, with increasing recycling rate *RC*, while similarity was quickly lost when recycling from reactor R stopped. Connected time points indicate the assembly trajectory of microbiomes. Points in gray represent samples from the other phases. The NMDS plots were created using relative cell numbers of all SCs based on Bray–Curtis distance measure (try = 100, trymax = 200). (*B*) Deviation of microbiome structure from the endpoints of respective previous phases (purple triangle) based on Canberra distance. The purple triangle in the Insular I phase represents the inoculum.

communities to remove carbon, phosphorus, and nitrogen remained fairly stable and even increased in the metacommunity setup.

Mass Transfer Synchronizes Microbiomes. The synchronization of microbiome structures between local communities L1–L5 and beyond with the regional pool was tested by calculating a range of diversity values (*SI Appendix*, section S8). With the exception of inventory α-diversity, we found that mass transfer strongly affected these values. All local microbiomes L1–L5 did not appreciably change in their richness during the 110 d of continuous cultivation, but γ-diversity, expressed as the richness of SCs in the metacommunity, was lowest at RC_{80} and highest in the Insular I and II phases (Table 1 and *SI Appendix*, Figs. S8.4 and S8.5), suggesting that the same SCs were dominating L1–L5 in phase 4 (RC_{80}).

Temporal intracommunity β-diversity values highlight structure variations per community. The highest values were found on day 3 for each of L1–L5 (35.8 ± 3.42), indicating rapid changes in L1–L5 during the adaptation period in the Insular I phase (Fig. 3*A*). For balanced periods within each phase, the intracommunity β-diversity values for the Insular I and II phases (8.63 ± 4.07 and 10.56 ± 4.86, respectively) and especially for RC_{50} and RC_{80} (5.56 ± 3.60 and 4.70 ± 2.52, respectively) were significantly lower (Table 1).

Temporal intracommunity β-diversity variations were also a means to find stochastic structural changes (i.e., drifts) in L1–L5 that occurred during the balanced periods under *RC*. If variations surpass a certain threshold, defined by the mean intracommunity β-diversity value that was determined for the balanced periods of the first phases of all L1–L5 (8.76, dashed lines in Fig. 3*A*), then they were considered drifts. Drifts were observed more frequently in the insular phases (Fig. 3*A* and *SI Appendix*, Tables S8.1 and S8.2) and were lowest for RC_{80}. Additionally, this synchrony at RC_{80} was even less deranged when looking at 16S rRNA gene sequencing data of sorted SCs (*SI Appendix*, Fig. S9.3). Some of the drifts could have been caused by different physiological cell states of dominant SCs (e.g., *Azospirillum* switching between six SCs with different growth states; *SI Appendix*, section S9), although the SCs could also comprise six different species or ecotypes. To quantify the relative contributions of deterministic and stochastic assembly processes in the local reactors, we used the approaches of Stegen et al. (38) and Ning et al. (39) based on our sequencing data and the approach of Ning et al. (40) based on our single-cell data. All three approaches, and in particular the normalized stochasticity ratio (NST) analysis, which showed a decrease in stochasticity to only 6% during RC_{80}, confirmed that the stochastic processes caused by dispersal limitation (in Insular I and II phases) were overcome by homogenizing dispersal processes during mass transfer (*SI Appendix*, section S14 and Figs. S14.1–S14.3). Stochastic changes in community structures thus appear to be significantly suppressed by mass transfer.

Intercommunity β-diversity was used to compare variations between L1–L5 and R at each time point. This diversity parameter was also highly sensitive to the recycling flow rate *RC* and significantly declined from the Insular I phase (19.58 ± 5.29) to RC_{80} (2.58 ± 1.65) and increased again in the Insular II phase (12.24 ± 5.20; Table 1 and Fig. 3*B*). The taxonomic composition of L1–L5 and R (genus level) was clearly different between the phases, with the exception of RC_{50} and RC_{80} (*SI Appendix*, Fig. S9.1), thus supporting the synchrony in microbiome compositions that was shown by the cytometric data.

Furthermore, the degree of exchange of particular SCs by other SCs, which is described by the term "turnover" β_{SIM}, was also high for the Insular I and II phases but only half as much for the RC_{80} (i.e., multisite intracommunity β-diversity; 0.34 ± 0.02; *SI Appendix*, Table S8.3). In contrast, "nestedness" β_{NES}, a value that describes the local and temporal persistence of SCs in communities (41), was highest at RC_{80} (0.14 ± 0.02; *SI Appendix*, Fig. S8.6*A* and Table S8.3). The type of the persistent SCs is presented in *SI Appendix*, Table S8.4. Thus, the strong compositional synchronization of the local microbiomes at RC_{80} was further supported by the determination of β_{SIM} and β_{NES} values, as the high turnover of SCs was observed only in the Insular I and II phases, but an increasing nestedness at RC_{80} (*SI Appendix*, Fig. S8.6*B* and Table S8.3).

Thus, although α-diversity richness values of local communities did not change, γ-diversity and intercommunity β-diversity were lowest at RC_{80}. At the end of RC_{80} (day 86), only 13 out of 80 SCs were dominating the final microbiomes in L1–L5 and R, with 54.7 to 65.6% of all cells in high synchrony. The intracommunity β-diversity indicated the lowest variation and lowest drift events at RC_{80}, which was also proven by whole-community 16S rRNA gene sequencing (*SI Appendix*, Fig. S9.1), for community trend analysis (*SI Appendix*, Fig. S9.2), and drift events (*SI Appendix*, Fig. S9.3). The 16S rRNA gene sequencing data supported and reinforced the cytometric data.

Mass Transfer Allows the Survival of Cells with a Low or Zero Net Growth Rate in Microbiomes. Subcommunities were found to survive in the reactors even when their net growth rate μ' was lower than the prevailing dilution rate $D = 0.72\ d^{-1}$.

The following ideal values for the mass transfer rate, M, were expected for the proposed experimental setup (*SI Appendix*, Figs. S10.1 and S10.2) when conditions assumed balanced situations (i.e., constant cell numbers) and when the cell numbers of the inflow (i.e., regional pool) were equal to cell numbers in the local microbiome. M should change with the recycling rate *RC*: $M = 0.072\ d^{-1}$ (RC_{10}), $M = 0.36\ d^{-1}$ (RC_{50}), and $M = 0.576\ d^{-1}$ (RC_{80}; *SI Appendix*, Eq. **S10.8**).

Table 1. Summary of α-diversity, γ-diversity, intracommunity β-diversity, intercommunity β-diversity (L vs. L), and intercommunity β-diversity (L vs. R) as mean ± SD per phase

Diversity/phase	Insular I	RC_{10}	RC_{50}	RC_{80}	Insular II
α-diversity	15.87 ± 4.42	15.84 ± 2.90	15.48 ± 1.71	15.52 ± 2.63	17.71 ± 3.18*
γ-diversity	39.73 ± 3.17***	31.00 ± 3.08	22.00 ± 2.73*	18.80 ± 3.85*	33.11 ± 3.62
Intracommunity β-diversity	8.63 ± 4.07	8.04 ± 3.65	5.56 ± 3.60	4.70 ± 2.52	10.56 ± 4.86
Intercommunity β-diversity (L vs. L)	19.58 ± 5.29***	13.58 ± 4.09	5.43 ± 3.36***	2.58 ± 1.65***	12.24 ± 5.20
Intercommunity β-diversity (L vs. R)	17.50 ± 4.23***	12.20 ± 3.58**	6.50 ± 3.03***	2.43 ± 1.82***	9.73 ± 4.54**

The mean ± SD values were all calculated among local microbiomes L1–L5 during balanced periods if not stated otherwise. The values marked with asterisks behind the diversity values in these phases were significantly different from those in any other phase. *$P \le 0.05$, **$P \le 0.01$, ***$P \le 0.001$.

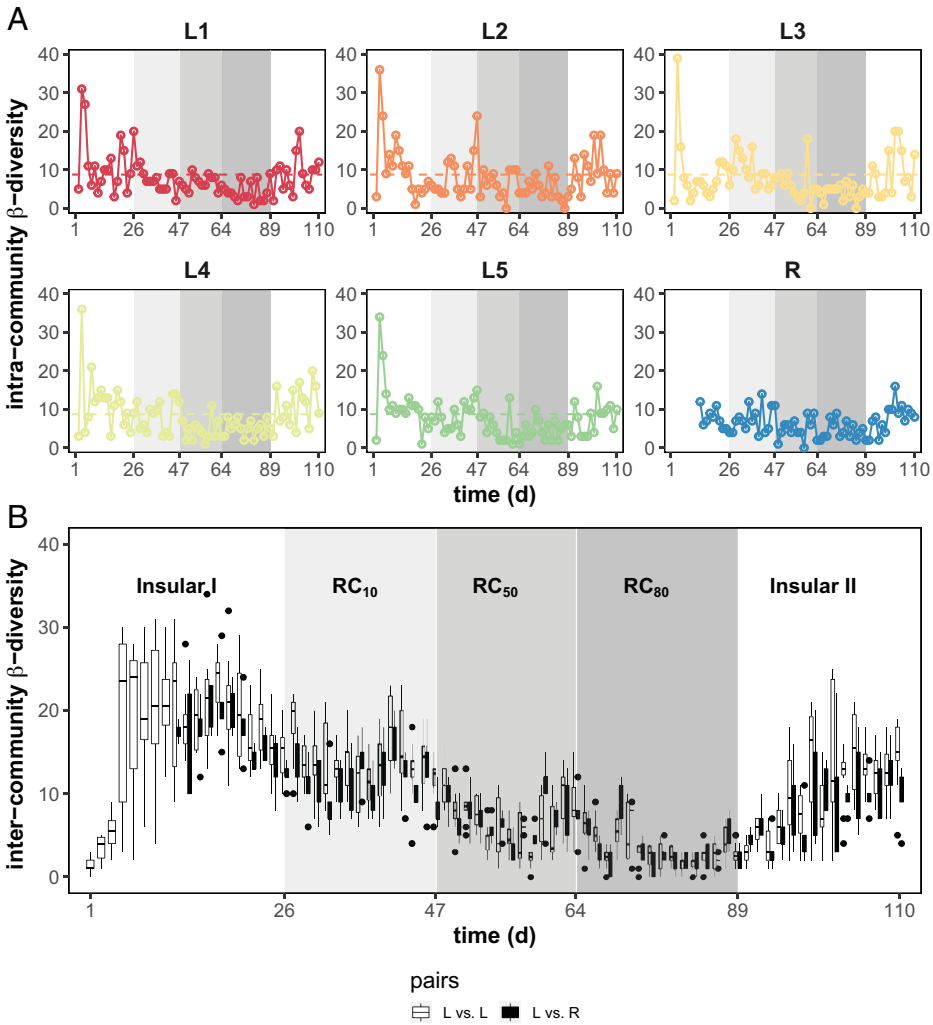

Fig. 3. Intra- and intercommunity β-diversity characteristics of local microbiomes L1–L5 and the regional pool R. (*A*) Variation of intracommunity β-diversity over time. The number of unique dominant SCs was determined in pairwise successive samples within a microbiome. The threshold value was 8.76 and used to distinguish drift events from intrinsic cellular fluctuations during balanced growth condition (horizontal dashed line). The intracommunity β-diversity values were reduced and showed fewer drift events under RC_{50} and RC_{80} conditions compared with other phases. (*B*) Variation of intercommunity β-diversity over time. Numbers of SCs were determined that were not shared in pairwise samples at the same time point between local microbiomes L vs. L (open symbols) and L vs. R (closed symbols). An increase in recycling rates *RC* lowered intercommunity β-diversity to a high degree. The shaded areas represent different phases with changes in *RC*.

Corresponding to $\mu' = D - M$ (*SI Appendix*, Eq. **S10.9**), the net growth rate can theoretically be calculated to be 0.648 d^{-1} (RC_{10}), 0.36 d^{-1} (RC_{50}), and 0.144 d^{-1} (RC_{80}; *SI Appendix*, Fig. S11.1*A*). The actual M values in the experiment closely followed the theoretical calculations (*SI Appendix*, Table S10.1), whereas the net growth rate μ' showed a few variations because of fluctuations in cell numbers (*SI Appendix*, Table S10.1 and Fig. S11.1*C*). These results demonstrate that at high *RC* and high M values the net growth rate μ' decreased sharply.

Similar to μ' for the whole community, the net growth rates of the subcommunities, $\mu' SC_x$, can be calculated (*SI Appendix*, Eqs. **S11.1–S11.5**). $\mu' SC_x$ decreased with increasing *RC*, partly to zero (Fig. 4, blue points), and the number of SCs in all local microbiomes with $\mu' SC_x \geq 0$ decreased from 305 out of 305 SCs in the Insular I phase to 124 out of 155 SCs at RC_{80} and increased back to 280 in the Insular II phase (*SI Appendix*, Fig. S11.1*D*). The number of SCs with $\mu' SC_x \geq 0$ per local microbiome at RC_{80} was similar to those in the regional pool R (23 SCs), which was much lower than the other phases (Fig. 4).

Subcommunities remained in the reactor setup at RC_{80} because of net growth in at least one of the five local microbiomes (Fig. 4, red points for L1–L5) and were rescued by their redistribution via the regional pool R. Some slow-growing or nongrowing SCs have also increased their abundance in the regional pool R (Fig. 4, red points for R). Some of the rescued SCs were cytometrically sorted and taxonomically sequenced. For example, at RC_{80}, *Azospirillum* (G33), *Azospira* (G18), and *Ochrobactrum* (G1; *SI Appendix*, Fig. S9.5) indicated net growth in all or most of the L1–L5 (Fig. 4, *SI Appendix*, section S9), whereas an unassigned genus from PeM15 (order, G12 and G14) accumulated in R, and cells of *Sphingobacteriaceae* (family, G4) and *Pseudacidovorax* (G2, G11; *SI Appendix*, Fig. S9.5) grew in few of the microbiomes L1–L5 and R and all were rescued by redistribution using R. These SCs were mainly monodominant and could be assumed to be superior local competitors under RC_{80} and R. Some other SCs that were also among the growing SCs (G5, G9, and G25; *SI Appendix*, Fig. S9.5 and Table S9.2) were multidominant. Generally, fewer SCs responded to mass transfer at RC_{80} but did so with higher relative abundance per SC (*SI Appendix*, Fig. S12.2). When performing correlations between absolute cell number per SC (*SI Appendix*, Fig. S8.2) and *RC*, five SCs

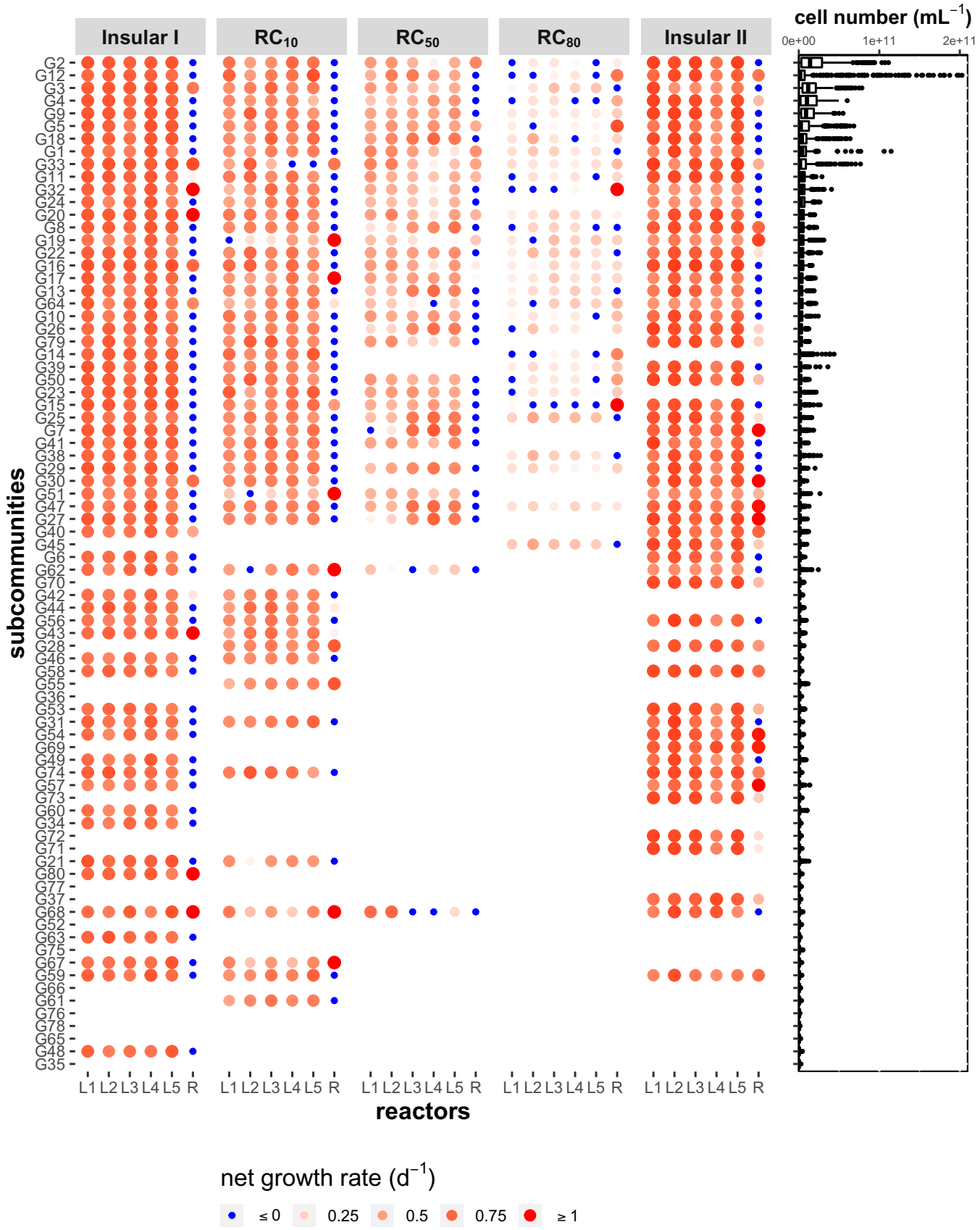

Fig. 4. Cell numbers of SCs and net growth rates $\mu' SC_x$ ($x = 1$ to 80), determined for the balanced periods of the different phases in the local communities L1–L5 and the regional pool (R). On the left, the net growth rate $\mu' SC_x$ (day^{-1}) is presented only for dominant SCs with relative abundances >1.25% in at least one sample during the corresponding periods in L1–L5 and R. The color gradient and size of the red circles represent the value of positive $\mu' SC_x$. Darker colors and larger circles indicate higher $\mu' SC_x$ values for positive net growth. All blue circles represent zero net growth $\mu' SC_x$. The SCs are ranked in descending order according to their mean cell number (cells per milliliter) for all days and all reactors. Cell numbers of $x = 80$ SCs of a total of 421 samples are shown as a boxplot on the right. Outliers of deviated cell number values are shown as points.

were revealed that all also showed net growth or rescue characteristics (G5, G12, G13, G14, and G33; *SI Appendix*, Fig. S12.1). Among the growing and rescued SCs were those that were nested. At RC_{80}, flow cytometrically determined nested SCs were G2, G4, G5, G9, G12, and G14 (*SI Appendix*, Table S8.4), and the 16S rRNA gene analysis determined *Pseudacidovorax* (G2), PeM15 (order, G12, G14), and multidominant G5 and G9 for these SCs (*SI Appendix*, Fig. S9.5).

Thus, the mass transfer supported genera that showed net growth $\mu' SC_x$ in at least one or a few of the local communities and were rescued by redistribution to all five communities through the regional pool R or accumulated in R and were also redistributed via R to the local communities. Subcommunities that exhibited net growth were also nested. These mechanisms ensured the survival of cells, even if they did not grow or grew more slowly in local microbiomes than the actual dilution rate D would allow.

Discussion

Stochasticity and dispersal are essential processes in shaping the structure and function of (meta)communities in natural environments, thereby influencing the ecological capacity and impact of microbial communities [e.g., Zhou et al. (42) and Wu et al. (43)]. Both random drift events, which influence the birth and death of organisms, and the extent to which organisms disperse are key factors in how communities are affected at local and temporal scales. According to Hubbell's (44) neutral theory, many natural patterns of community assembly can only be explained by these neutral events, in which niche-based selection is accompanied by random immigration and emigration, resulting in ecological drifts and a metacommunity formed by dispersal (45). Through experimentation and analogy, ecological drifts have been shown to be greater when abiotic niches are shallow, competition is weak, and dispersal is low (46–48).

The absence of dispersal results in communities that are isolated from each other, making them susceptible to stochastic variation (9, 10, 13). Low dispersal is common in macroecology and contributes to the presence and coexistence of multiple species within a metacommunity of multiple patches (49, 50). In contrast, high dispersal is known to increase similarity between localities and thus the risk of global extinction (51–53). High dispersal has a quantitative effect on local community formation in accordance to the mass-effect paradigm, in which community composition in sink habitats tends to resemble that of the source habitat (44, 54). Frequently, the abundance of species in source communities and their transfer rates influence the composition of sink habitats (55), and lost individuals are replaced by members of source communities (56). This underscores the assumption that a regional pool that floods local communities with high rates of mass transfer can lead to synchrony and stability. Usually, mass transfer occurs between ecologically distinct niches in natural and engineered systems. Even when mass transfer is high, different environments have specific community structures, e.g. discrete bacterioplankton communities in a lake and its inlets (32) or microbial communities in connected transects of wastewater treatment plants (26, 37).

In the metacommunity of this study, identical localities operated in the same way were also expected to develop disparity (9), but these were overcome by the loop design. The looped mass transfer between the five local reactors L1–L5 and the regional pool R minimized the ability to form independent and disparate microenvironments. Separate local niches that originally formed during the first 26 d of insular setup elapsed. After, the microbiomes in L1–L5 and R formed a mutual niche where the same core microbiomes always dominated (*SI Appendix*, Fig. S12.2). These metacommunity niche-shaping effects were major events that caused the transitional loss of cell types that were previously dominant in the insular phase. Our study demonstrated that the invented loop-designed mass transfer significantly switched the community assembly from the dispersal limitation to a homogenous dispersal process (*SI Appendix*, section S14; NST, 40; QPEN, 38; iCAMP, 39), thereby stabilizing the microbiomes and increasing the synchrony between the six localities.

It should be noted that while experiments which are designed to compare different treatments often focus on effect size and significance and therefore require a certain number of replicates, in our case stabilization of community structure and function, as compared to isolated reactors as in Liu et al. (9), has been demonstrated by a wide range of metrics, addressing different aspects of the community, all based on single-cell data, building on an analysis of about 90 million cells. More extensive studies, either tracking thousands of generations, as shown for example by the Lenski group (57) for pure populations, or involving multiple independent and parallel metacommunities, could further verify the results due to even higher sample density and the repetitive experimental design. Nevertheless, studying a community for a minimum of 114 generations under balanced continuous growth conditions allowed us to determine the basic properties of the community under successive changes in mass transfer rates. These were stability properties, diversity metrics, net growth rates of subcommunities, proportions of stochastic and deterministic processes, and the rescue of cell types at high mass transfer, creating communities that remain unchanged in composition and function.

The metric "stability" is described by various properties, out of which constancy, resistance, and recovery are the most essential ones (1). We found greater constancy and resistance values in L1–L5 at RC_{50} and RC_{80}, reflecting stability of the community to stochastic assembly processes and perturbation events (i.e., dilution rate). The source–sink relationship between L1–L5 and the regional pool R created a reduction of the species pool but at high cell abundance that provided less space for neutral forces. Long-term constancy was established when transfer rates at RC_{50} and RC_{80} prevented the extinction of local species through the rescue effect and when regional equality was achieved according to Chesson (58). The increase in resistance that was observed in the present study could also be the result of the gradual increase in mass transfer rates (i.e., the RC_{10} phase selected already partially nested SCs that eventually dominated at RC_{50} and RC_{80}, such as G2; *SI Appendix*, Table S8.4). Recovery by definition describes the ability of a community to return to the constancy space after a temporary disturbance (1, 2). We found that recovery values were always low because the microbiomes were intentionally steered toward a low-diverse but unchanging state through the use of the loop-designed metacommunity setup. Nonetheless, recovery values were always positive, despite permanent changes in mass transfer rates and because of reinforcement of the rescue effect, which, in addition to the high constancy and resistance values, demonstrates the high stability properties of the metacommunity at RC_{50} and RC_{80}. Nevertheless, we would like to point out that very long-lasting mass transfer rates could still lead to slow, transient changes in microbial community structure, as Francis et al. (59) predicted for macroecological systems, but we always would expect synchrony to be maintained in local

communities. The functions of the wastewater community, i.e., high carbon, ammonium-nitrogen, and phosphorus removal efficiencies and biomass production, were always active in both L1–L5 and R and were not lost even as mass transfer rates increased (*SI Appendix*, section S3). For carbon and ammonium we even found an increase in removal efficiency with mass transfer rates in the metacommunity setup due to repeated recycling of the compounds in the flow, suggesting that the functions of the wastewater community to remove carbon, nitrogen, and phosphorus were at least stabilized if not increased. Notably, relief from mass transfer restored efficiencies to near starting values and also led to a renewal of earlier diversity levels (Insular I phase vs. Insular II phase), indicating that rare species were still present to allow diversity to return.

By using various diversity metrics we found that high mass transfer rates affected diversity values and reinforced specific cell types. Looped high mass transfer did not alter richness in terms of number of dominant SCs or individual cell production per reactor much (PC; *SI Appendix*, Table S10.1), but it reduced β-diversity between and within microbiomes and resulted in the loss of local niches, which in turn reduced γ-diversity (Table 1). As a consequence of the lower number of cell types, high mass transfer resulted in lower stochastic drift events (*SI Appendix*, Table S8.1) and thus narrower established constancy spaces (Fig. 2*B*). Fewer or even no drift events were found in the balanced growth periods, indicating that neutral forces in the metacommunity were low, differing from insular environments (9, 10). Random birth and death events were limited by the continuous inflow of source organisms from the regional pool R and by the increase in biomass with increasing mass transfer (*SI Appendix*, Fig. S3.1). High biomass is known to lower susceptibility to demographic drift or disturbance (60).

Another argument in favor of the power of mass transfer to prevent variation was the low degree of the exchange, β_{SIM} (turnover), of SCs within and between microbiomes at high mass transfer rates, which was different for insular situations (*SI Appendix*, Fig. S8.6 and Table S8.3). Conditions of strong mass transfer have been described to moderate the turnover of community structures and support the nestedness of species, e.g. in the process of biotic homogenization (61) or postglacial recolonization processes of northern biotopes (62). Most SCs that benefitted from mass transfer were also those that showed persistence, β_{NES} (nestedness; *SI Appendix*, Table S8.4). Similar to core species, they could also play an important role in maintaining community traits. Core species are common and dominant, e.g. in gut microbiomes (63), in benthic octocoral associations in the form of symbiosis (64), and species in macroecology that cope with climate warming, which largely determines temporal stability of the total biomass in alpine grassland communities (65). A huge number of technologies are available to recognize core species and, moreover, to determine their functions, as recently reviewed by Hatzenpichler et al. (66). However, our study did not focus on the functional activity of individual cells. Nevertheless, we were able to decipher some of the most persistent cell types and their functional capacity through correlation analyses combined with cell sorting and 16S rRNA gene sequencing. In our loop design, dominant SCs indicated an increased number of correlations despite nutrient limitation that was caused by high cell density during RC_{50} and RC_{80} in L1–L5 and especially in the regional pool R (*SI Appendix*, Table S13.1). Genera in nested SCs were able to survive in R (*SI Appendix*, Table S8.4) because they could potentially cope with the low carbon and ammonium resources, such as *Sphingobacteriaceae* (*SI Appendix*, Fig. S9.1) (67–69) or PeM15 (70). Nested *Azospirillum* (G33), *Azospira* (G18), and *Pseudacidovorax* (G2, G11; *SI Appendix*, Fig. S9.5) are nitrogen fixers. They may have displaced other genera because of ammonium self-sufficiency (71–73). Thus, the regional pool R might have acted as a "hotspot" for genus and function selection, which underscores the possibility of selecting desired functions by modifying the conditions of the regional pool.

We also found that mass transfer supported slow-growing organisms through the rescue effect. Mass transfer is a source–sink relationship and contributes to the spread and survival of species in sinks that would otherwise go extinct (74). Source–sink relationships are generally very strong to ensure coexistence, and modeled environmental variations were found to not affect them (75–77). The rescue of species at a sink site is reflected in various biotechnological processes where biotechnologists have successfully used this source–sink principle for bio-augmentation to keep a desired species in a system (78, 79).

Most studies, however, ignore or cannot distinguish between the niche-specific competitive hierarchy of microbiome members in sources or sinks and the effects of emigration and immigration on these relationships. Recent studies have begun to track sink members within microbiomes by calculating their net growth based on the relative abundances of 16S rRNA gene sequencing data and bulk biomass to approximate their contribution to sink biomass formation (80, 81). Our study goes a step further by implementing net growth metrics for all cell types that migrated back and forth within the loop-designed source–sink metacommunity, based on data from individual cells.

We found that slow-growing or almost nongrowing cell types, which would typically be washed-out under continuous feeding conditions (9), remained part of the microbiome through the rescue effect (Fig. 4). At the extreme, at RC_{80}, when the metacommunity was fully mixed and when the final microbiome was established, the growth of some SCs in L1–L5 was especially low or nonexistent because of an increase in biomass and decrease in nutrient resources. However, these SCs overcame their nongrowth in one or two reactors by growing in one or more of the other five local reactors and, subsequently, by redistribution via R, which enhanced their persistence in the metacommunity. Similar rescue effects were modeled for a macroecology background in relation to a metafood web, suggesting that biodiversity can be buffered under global change (82). The source–sink relationship from local communities L1–L5 to the regional pool R and its reverse loop supported the growth of SCs in L1–L5 rather than in nutrient-limited R. Unknown is why cells were nested in R and rescued through R. The few SCs (e.g., multidominant G5 and PeM15 in G12, G14) showed small cell morphologies. It is conceivable that they might have been able to successfully utilize the limited resources and simultaneously take advantage of the high-exchange-rate ($D = 3.6\ d^{-1}$) qualities of R.

Our setup was thus able to protect slow-growing or even nongrowing microorganisms for at least 114 generations, which otherwise would not have survived without mass transfer and the rescue effect. The loop-designed metacommunity may thus be a tool to protect and preserve functionally valuable microorganisms even if their growth rate is slow and lower than the prevailing dilution rate.

In summary, looped mass transfer is a means of stabilizing microbial communities over long periods of time. The degree of stabilization can be selected via the mass transfer rate *RC*.

Mass transfer reduced local and temporal variations, and the stochastic behavior that is normally observed in insular setups was reduced. All microbiomes showed high constancy and increasing resistance as well as unaffected functions at high mass transfer rates. Mass transfer also synchronized structures of the microbiomes by the mechanism of homogeneous dispersal, resulting in the lowest intercommunity β-diversity at the highest mass transfer. The variation of β-diversity within communities ceased, and the persistence of particular SCs was highest at high mass transfer. High turnover of community structures was observed only when no mass transfer occurred. An increase in mass transfer also increased cell numbers, thereby decreasing net growth rates μ'. Subcommunities that showed no growth ($\mu' SC_x = 0$) in one locality were rescued by growth at another locality and by their redistribution via the loop design. Thus, lost SCs, whose growth rate was below the dilution rate and that would normally go extinct, were fostered and replaced by members of the source community. The regional pool itself also served as a rescue site through the redistribution of SCs that accumulated specifically in R.

The local reactor conditions that were used in this study ultimately selected our microbiome. It is conceivable to test other local and especially regional conditions that support other cell types in natural communities in the future and thus design other stabilized communities. In particular, when certain medically or biotechnologically relevant functions are desired that require organisms with different physiological properties, including different growth rates, our loop design provides a solution for long-term stabilization and thus the reliable functioning of microbiomes.

Materials and Methods

The metacommunity consisted of five local communities (L1–L5) that were operated in parallel and identically in continuous-flow reactors (Fig. 1). To establish mass transfer between L1–L5, effluents from all five bioreactors were combined in a sixth bioreactor (i.e., the regional pool R). After mixing, a part of the regional pool R was returned to L1–L5 via a recycling loop.

In accordance with Liu et al. (9), the cultivation of L1–L5 began simultaneously with an identical inoculum that originated from a full-scale wastewater treatment plant (*SI Appendix*, section S1). To study the effects of mass transfer, recycling flow rates *RC* were applied with 10% (RC_{10}), 50% (RC_{50}), and 80% (RC_{80}) of the original medium feeding rate of 0.4 mL·min^{-1} (*SI Appendix*, section S2).

The experiment was run for 110 d. Five phases were distinguished in accordance to their recycling flow rate *RC*: phase 1 with no recycling (Insular I, starting on day 0), phases 2 to 4 (with recycling flow rates RC_{10}, RC_{50}, and RC_{80}, starting on days 26, 47, and 64, respectively), and phase 5 (Insular II, starting on day 89), again without recycling. Within each phase, the first 7 d (five times volume exchange of a reactor) were defined as the adaptation period, and the subsequent days were a balanced period during which abiotic parameters were expected to be more or less constant (*SI Appendix*, section S3).

A total of 448 samples were collected from the six bioreactors, (i.e., 76 samples from each of the five local communities L1–L5 and 68 samples from the regional pool R; *SI Appendix*, section S3 and Dataset S1). The harvested cells were stabilized, stored at −20 °C, and stained with 4′,6-diamidino-2-phenylindole (DAPI) for flow cytometric measurement (*SI Appendix*, section S4). The samples were analyzed with a MoFlo Legacy Cell Sorter (Beckman Coulter). To ensure reliability of the cell handling procedures, a microbial cytometric mock community (83) was used, which was handled identically to the reactor samples on each measurement day. The instrument was optically aligned daily using 0.5-μm and 1-μm ultraviolet monodisperse fluorescent beads, and the same beads were inserted into each sample as an internal reference to monitor the instrument's stability (*SI Appendix*, section S4). All raw data are available in the FlowRepository (https://flowrepository.org/; accession no. FR-FCM-Z3MU).

Single-cell data were collected in logarithmically scaled two-dimensional (2D) dot plots of DAPI fluorescence vs. forward scatter for cell-size-related information. A cell gate that excluded beads and noise was defined, which included 200,000 virtual cells for each measurement. According to apparent cell clusters in the 2D dot plots of all measured samples (n = 448), a gate-template with 80 gates was defined (G1–G80). The cell gate, the cell numbers per gate of the gate template, and the measured total cell number (CN) were used to determine both the relative and absolute cell numbers per gate over time (*SI Appendix*, Figs. S8.1–S8.3). In this study, we refer to the cells from a gate (G) as a subcommunity (SC). Data from a total of 35,840 SCs (including 80 SCs of the inoculum) were obtained (*SI Appendix*, section S4 and Dataset S2). Dominant SCs were defined as having an average proportion of cell numbers higher than 1.25%.

For cell counting, live cells were stained with SYTO9 and counted flow cytometrically with the CyFlowSpace (Sysmex Partec GmbH) by using the True Volumetric Absolute Counting mode and FloMax 2.4 (Sysmex Partec; *SI Appendix*, section S5).

A total of 500,000 cells of each selected SC were sorted, and the cell pellets were stored at −20 °C for subsequent DNA isolation (*SI Appendix*, section S4). DNA from both whole-community samples and sorted cells was extracted (*SI Appendix*, section S6). The 16S rRNA gene amplicon sequencing was performed by using Pro341F (84) and Pro805R (85) primers for the V3-V4 region. To ensure quality of the sequencing run and analysis, a sequencing mock community (ZymoBIOMICS Microbial Community Standard; Zymo Research) was included in the sequencing project (*SI Appendix*, Fig. S6.1). The community and SC samples were resolved at the genus level (*SI Appendix*, Figs. S9.1 and S9.5). All raw data are available in the NCBI Sequence Read Archive (https://www.ncbi.nlm.nih.gov/bioproject/PRJNA756026/; accession no. PRJNA756026). All tools and scripts that were used for the statistical analyses are provided in *SI Appendix*, section S6, step 6.

Changes in microbiome structures were visualized by dissimilarity analysis (Bray–Curtis index) based on relative cell abundance per SC (*SI Appendix*, section S8, step 1). The temporal variation in community structure was quantified by calculating Canberra distances from the endpoints of respective previous phases to each of the subsequent relative cell numbers per SC (*SI Appendix*, section S7, step 1). Effluents between local communities L1–L5 and the regional pool R were compared by permutational analysis of variance (PERMANOVA) to test whether L1–L5 alone structured the R community (*SI Appendix*, section S8, step 2).

Intra- and intercommunity β-diversity were calculated to quantify temporal and regional variations of the local microbiomes L1–L5 and regional pool R (9). Community inherent stochastic drift events were highlighted based on intracommunity β-diversity values. Changes in α- and γ-diversity values were also documented (*SI Appendix*, section S8, step 3). The relative proportions of deterministic and stochastic processes that influenced the assembly of the communities from dispersal limitation in the Insular I phase (and back in the Insular II phase) to a homogenous dispersal process during mass transfer were calculated using the tools described in *SI Appendix*, section S14.

To quantify the increasing synchrony in SC emergence in the reactors, community composition variation was partitioned into species replacement and species loss to determine turnover and nestedness using a method that was developed for microbial community flow cytometric data. The turnover β_{SIM} and nestedness β_{NES} components of Sørensen dissimilarity were calculated (61, 62) (*SI Appendix*, section S8, step 4).

To understand the effect of mass transfer on diversity patterns and synchrony, we calculated the net growth rate of both the entire microbiomes (μ'; *SI Appendix*, section S10) and every dominant SCs in local microbiomes L1–L5 ($\mu' SC_x$; *SI Appendix*, section S11). The net growth rates were calculated from cell numbers in the inflow, cell numbers lost by the effluent, and the growth of cells in a time interval Δt (d) (*SI Appendix*, section S10 and Eqs. **S10.1**-**S10.10** and **S11.1**-**S11.5**).

To verify synchrony with increasing recycling flow rates *RC*, stability properties (2) were calculated for the whole communities (*SI Appendix*, section S7) and highlighted for SCs that were promoted by mass transfer (*SI Appendix*, section S12).

Data Evaluation. Unless otherwise noted, all calculations and analyses were performed using RStudio v1.2.1335 with R v3.6.3. The dissimilarity analysis was supported by the R packages vegan v2.5.6 (86) and flowCyBar (87) (http://

bioconductor.org/packages/flowCyBar/). The correlation analysis and the partial Mantel test were supported by the R packages Hmisc v4.4.0 (88) and vegan v2.5.6 (86). The quantification of stability properties followed the R script of Liu et al. (2). Detailed descriptions of the statistical handling are provided in *SI Appendix*: stability test (*SI Appendix*, section S7), community composition analysis (*SI Appendix*, section S8), sequencing-data-based analysis (*SI Appendix*, section S9), net growth rates (*SI Appendix*, sections S10 and S11 and Datasets S6 and S7), and correlation analysis (*SI Appendix*, sections S12 and S13), respectively. The Wilcoxon test was conducted to determine significance ($P < 0.05$) of the difference in α-, β-, and γ-diversity values, numbers of correlations, and stability property values between pairwise phases. The PERMANOVA test was supported by R package vegan v2.5.6 (86). The graphical work was supported by the R package ggplot2 v3.3.0 (89).

Data Availability. Flow cytometric raw data, 16S rRNA gene amplicon sequencing data, and R scripts and materials for data analysis and relevant graphical work have been deposited in FlowRepository (accession no. FR-FCM-Z3MU), NCBI Sequence Read Archive (accession no. PRJNA756026), and GitHub (https://github.com/ufzshuangli/mc_masstransfer).

ACKNOWLEDGMENTS. This work was funded by the European Regional Development Funds (EFRE–Europe Funds Saxony, Grant 100192205) and the Helmholtz Association, Helmholtz-Centre for Environmental Research – UFZ in the frame of the Integrated Platform Electro-Biorefineries & Biosyntheses. The work was also supported by the Chinese Scholarship Council, the Petroleum Technology Development Fund, and the German Academic Exchange Service (ID 57401043).

Author affiliations: [a]Department of Environmental Microbiology, Helmholtz Centre for Environmental Research – UFZ, 04318 Leipzig, Germany; [b]Department of Ecological Modelling, Helmholtz Centre for Environmental Research – UFZ, 04318 Leipzig, Germany; [c]Plant Ecology and Nature Conservation, University of Potsdam, 14476 Potsdam, Germany; and [d]College of Environmental and Resource Sciences, Zhejiang University, Hangzhou 310058, China

1. V. Grimm, C. Wissel, Babel, or the ecological stability discussions: An inventory and analysis of terminology and a guide for avoiding confusion. *Oecologia* **109**, 323–334 (1997).
2. Z. Liu *et al.*, Ecological stability properties of microbial communities assessed by flow cytometry. *MSphere* **3**, e00564-17 (2018).
3. H. Weise *et al.*, Resilience trinity: Safeguarding ecosystem functioning and services across three different time horizons and decision contexts. *Oikos* **129**, 445–456 (2020).
4. L. T. Angenent, J. A. Magdalena, B. S. Jeon, J. G. Usack, Eco-mimicry opens new doors for bioprocess engineers. *Joule* **4**, 2074–2077 (2020).
5. K. D'Hondt *et al.*, Microbiome innovations for a sustainable future. *Nat. Microbiol.* **6**, 138–142 (2021).
6. C. E. Lawson *et al.*, Common principles and best practices for engineering microbiomes. *Nat. Rev. Microbiol.* **17**, 725–741 (2019).
7. D. Rodríguez Amor, M. Dal Bello, Bottom-up approaches to synthetic cooperation in microbial communities. *Life (Basel)* **9**, 22 (2019).
8. S. Fodelianakis *et al.*, Dispersal homogenizes communities via immigration even at low rates in a simplified synthetic bacterial metacommunity. *Nat. Commun.* **10**, 1314 (2019).
9. Z. Liu *et al.*, Neutral mechanisms and niche differentiation in steady-state insular microbial communities revealed by single cell analysis. *Environ. Microbiol.* **21**, 164–181 (2019).
10. R. Liébana *et al.*, Combined deterministic and stochastic processes control microbial succession in replicate granular biofilm reactors. *Environ. Sci. Technol.* **53**, 4912–4921 (2019).
11. C.-M. Klask, N. Kliem-Kuster, B. Molitor, L. T. Angenent, Nitrate feed improves growth and ethanol production of *Clostridium ljungdahlii* with CO_2 and H_2, but results in stochastic inhibition events. *Front. Microbiol.* **11**, 724 (2020).
12. C. Y. Chang *et al.*, Engineering complex communities by directed evolution. *Nat. Ecol. Evol.* **5**, 1011–1023 (2021).
13. J. Zhou *et al.*, Stochastic assembly leads to alternative communities with distinct functions in a bioreactor microbial community. *MBio* **4**, e00584-12 (2013).
14. L. G. Shoemaker *et al.*, Integrating the underlying structure of stochasticity into community ecology. *Ecology* **101**, e02922 (2020).
15. F. Jeltsch, V. Grimm, J. Reeg, U. E. Schlagel, Give chance a chance: From coexistence to coviability in biodiversity theory. *Ecosphere* **10**, e02700 (2019).
16. J. Zhou, D. Ning, Stochastic community assembly: Does it matter in microbial ecology? *Microbiol. Mol. Biol. Rev.* **81**, e00002–e00017 (2017).
17. M. Vellend, Conceptual synthesis in community ecology. *Q. Rev. Biol.* **85**, 183–206 (2010).
18. D. R. Nemergut *et al.*, Patterns and processes of microbial community assembly. *Microbiol. Mol. Biol. Rev.* **77**, 342–356 (2013).
19. J. C. Stegen, X. Lin, A. E. Konopka, J. K. Fredrickson, Stochastic and deterministic assembly processes in subsurface microbial communities. *ISME J.* **6**, 1653–1664 (2012).
20. P. V. Fine, S. W. Kembel, Phylogenetic community structure and phylogenetic turnover across space and edaphic gradients in western Amazonian tree communities. *Ecography* **34**, 552–565 (2011).
21. Q. Yan *et al.*, Nearly a decade-long repeatable seasonal diversity patterns of bacterioplankton communities in the eutrophic Lake Donghu (Wuhan, China). *Mol. Ecol.* **26**, 3839–3850 (2017).
22. Z. Zhang *et al.*, Deterministic assembly and diversity gradient altered the biofilm community performances of bioreactors. *Environ. Sci. Technol.* **53**, 1315–1324 (2019).
23. W. Xun *et al.*, Diversity-triggered deterministic bacterial assembly constrains community functions. *Nat. Commun.* **10**, 3833 (2019).
24. R. E. Danczak *et al.*, Using metacommunity ecology to understand environmental metabolomes. *Nat. Commun.* **11**, 6369 (2020).
25. B. J. McGill *et al.*, Species abundance distributions: Moving beyond single prediction theories to integration within an ecological framework. *Ecol. Lett.* **10**, 995–1015 (2007).
26. S. Günther *et al.*, Species-sorting and mass-transfer paradigms control managed natural metacommunities. *Environ. Microbiol.* **18**, 4862–4877 (2016).
27. A. K. Dewdney, *Stochastic Communities: A Mathematical Theory of Biodiversity* (CRC Press, Boca Raton, FL, 2017).
28. N. A. Cutler, D. L. Chaput, A. E. Oliver, H. A. Viles, The spatial organization and microbial community structure of an epilithic biofilm. *FEMS Microbiol. Ecol.* **91**, fiu027 (2015).
29. S. J. Bent, L. J. Forney, The tragedy of the uncommon: Understanding limitations in the analysis of microbial diversity. *ISME J.* **2**, 689–695 (2008).
30. I. Hanski, *Metapopulation Ecology* (Oxford University Press, 1999).
31. M. A. Leibold *et al.*, The metacommunity concept: A framework for multi-scale community ecology. *Ecol. Lett.* **7**, 601–613 (2004).
32. J. B. Logue, E. S. Lindström, Species sorting affects bacterioplankton community composition as determined by 16S rDNA and 16S rRNA fingerprints. *ISME J.* **4**, 729–738 (2010).
33. J. G. Wu, O. L. Loucks, From balance of nature to hierarchical patch dynamics: A paradigm shift in ecology. *Q. Rev. Biol.* **70**, 439–466 (1995).
34. A. Shmida, M. V. Wilson, Biological determinants of species-diversity. *J. Biogeogr.* **12**, 1–20 (1985).
35. J. H. Brown, A. Kodricbrown, Turnover rates in insular biogeography–Effect of immigration on extinction. *Ecology* **58**, 445–449 (1977).
36. Y. Zha, E. S. Lindström, A. Eiler, R. Svanbäck, Different roles of environmental selection, dispersal, and drift in the assembly of intestinal microbial communities of freshwater fish with and without a stomach. *Front. Ecol. Evol.* **8**, 152 (2020).
37. V. Vučić, C. Süring, H. Harms, S. Müller, S. Günther, A framework for P-cycle assessment in wastewater treatment plants. *Sci. Total Environ.* **760**, 143392 (2021).
38. J. C. Stegen *et al.*, Quantifying community assembly processes and identifying features that impose them. *ISME J.* **7**, 2069–2079 (2013).
39. D. Ning *et al.*, A quantitative framework reveals ecological drivers of grassland microbial community assembly in response to warming. *Nat. Commun.* **11**, 4717 (2020).
40. D. Ning, Y. Deng, J. M. Tiedje, J. Zhou, A general framework for quantitatively assessing ecological stochasticity. *Proc. Natl. Acad. Sci. U.S.A.* **116**, 16892–16898 (2019).
41. Z. Liu, S. Müller, Bacterial community diversity dynamics highlight degrees of nestedness and turnover patterns. *Cytometry A* **97**, 742–748 (2020).
42. J. Zhou *et al.*, Stochasticity, succession, and environmental perturbations in a fluidic ecosystem. *Proc. Natl. Acad. Sci. U.S.A.* **111**, E836–E845 (2014).
43. L. Wu *et al.*; Global Water Microbiome Consortium, Global diversity and biogeography of bacterial communities in wastewater treatment plants. *Nat. Microbiol.* **4**, 1183–1195 (2019).
44. S. P. Hubbell, *The Unified Neutral Theory of Biodiversity and Biogeography (MPB-32)* (Princeton University Press, 2011).
45. J. M. Chase, Drought mediates the importance of stochastic community assembly. *Proc. Natl. Acad. Sci. U.S.A.* **104**, 17430–17434 (2007).
46. J. M. Chase, Community assembly: When should history matter? *Oecologia* **136**, 489–498 (2003).
47. J. M. Chase, Stochastic community assembly causes higher biodiversity in more productive environments. *Science* **328**, 1388–1391 (2010).
48. J. M. Chase, J. A. Myers, Disentangling the importance of ecological niches from stochastic processes across scales. *Philos. Trans. R. Soc. Lond. B Biol. Sci.* **366**, 2351–2363 (2011).
49. F. Altermatt, V. I. Pajunen, D. Ebert, Climate change affects colonization dynamics in a metacommunity of three *Daphnia* species. *Glob. Change Biol.* **14**, 1209–1220 (2008).
50. S. A. Declerck, C. Winter, J. B. Shurin, C. A. Suttle, B. Matthews, Effects of patch connectivity and heterogeneity on metacommunity structure of planktonic bacteria and viruses. *ISME J.* **7**, 533–542 (2013).
51. B. Ashby, A. K. Shaw, H. Kokko, An inordinate fondness for species with intermediate dispersal abilities. *Oikos* **129**, 311–319 (2020).
52. K. C. Abbott, A dispersal-induced paradox: Synchrony and stability in stochastic metapopulations. *Ecol. Lett.* **14**, 1158–1169 (2011).
53. S. Gokhale, A. Conwill, T. Ranjan, J. Gore, Migration alters oscillatory dynamics and promotes survival in connected bacterial populations. *Nat. Commun.* **9**, 5273 (2018).
54. W. T. Sloan, S. Woodcock, M. Lunn, I. M. Head, T. P. Curtis, Modeling taxa-abundance distributions in microbial communities using environmental sequence data. *Microb. Ecol.* **53**, 443–455 (2007).
55. R. J. Stoffels, K. R. Clarke, D. S. Linklater, Temporal dynamics of a local fish community are strongly affected by immigration from the surrounding metacommunity. *Ecol. Evol.* **5**, 200–212 (2015).
56. S. Woodcock, W. T. Sloan, Biofilm community succession: A neutral perspective. *Microbiology (Reading)* **163**, 664–668 (2017).
57. B. H. Good, M. J. McDonald, J. E. Barrick, R. E. Lenski, M. M. Desai, The dynamics of molecular evolution over 60,000 generations. *Nature* **551**, 45–50 (2017).
58. P. Chesson, Mechanisms of maintenance of species diversity. *Annu. Rev. Ecol. Syst.* **31**, 343–366 (2000).
59. T. B. Francis *et al.*, Management implications of long transients in ecological systems. *Nat. Ecol. Evol.* **5**, 285–294 (2021).
60. M. E. Yeager, T. C. Gouhier, A. R. Hughes, Predicting the stability of multitrophic communities in a variable world. *Ecology* **101**, e02992 (2020).
61. L. Baeten *et al.*, Distinguishing between turnover and nestedness in the quantification of biotic homogenization. *Biodivers. Conserv.* **21**, 1399–1409 (2012).
62. A. Baselga, Partitioning the turnover and nestedness components of beta diversity. *Glob. Ecol. Biogeogr.* **19**, 134–143 (2010).
63. P. J. Turnbaugh, J. I. Gordon, The core gut microbiome, energy balance and obesity. *J. Physiol.* **587**, 4153–4158 (2009).

64. J. A. J. M. van de Water *et al.*, Seasonal stability in the microbiomes of temperate gorgonians and the red coral *Corallium rubrum* across the Mediterranean sea. *Microb. Ecol.* **75**, 274–288 (2018).
65. Z. Ma *et al.*, Climate warming reduces the temporal stability of plant community biomass production. *Nat. Commun.* **8**, 15378 (2017).
66. R. Hatzenpichler, V. Krukenberg, R. L. Spietz, Z. J. Jay, Next-generation physiology approaches to study microbiome function at single cell level. *Nat. Rev. Microbiol.* **18**, 241–256 (2020).
67. S. Nagar *et al.*, Phylogenetic relationships and potential functional attributes of the genus *Parapedobacter*: A member of family *Sphingobacteriaceae*. *Front. Microbiol.* **11**, 1725 (2020).
68. P. L. Steyn *et al.*, Classification of heparinolytic bacteria into a new genus, *Pedobacter*, comprising four species: *Pedobacter heparinus* comb. nov., *Pedobacter piscium* comb. nov., *Pedobacter africanus* sp. nov. and *Pedobacter saltans* sp. nov. proposal of the family *Sphingobacteriaceae* fam. nov. *Int. J. Syst. Bacteriol.* **48**, 165–177 (1998).
69. T. A. Pankratov, B. J. Tindall, W. Liesack, S. N. Dedysh, *Mucilaginibacter paludis* gen. nov., sp. nov. and *Mucilaginibacter gracilis* sp. nov., pectin-, xylan- and laminarin-degrading members of the family *Sphingobacteriaceae* from acidic *Sphagnum* peat bog. *Int. J. Syst. Evol. Microbiol.* **57**, 2349–2354 (2007).
70. H. F. Arocha-Garza, R. Canales-Del Castillo, L. E. Eguiarte, V. Souza, S. De la Torre-Zavala, High diversity and suggested endemicity of culturable *Actinobacteria* in an extremely oligotrophic desert oasis. *PeerJ* **5**, e3247 (2017).
71. O. Steenhoudt, J. Vanderleyden, *Azospirillum*, a free-living nitrogen-fixing bacterium closely associated with grasses: Genetic, biochemical and ecological aspects. *FEMS Microbiol. Rev.* **24**, 487–506 (2000).
72. H. S. Bae *et al.*, Description of *Azospira restricta* sp. nov., a nitrogen-fixing bacterium isolated from groundwater. *Int. J. Syst. Evol. Microbiol.* **57**, 1521–1526 (2007).
73. P. Kämpfer *et al.*, *Pseudacidovorax intermedius* gen. nov., sp. nov., a novel nitrogen-fixing betaproteobacterium isolated from soil. *Int. J. Syst. Evol. Microbiol.* **58**, 491–495 (2008).
74. T. N. Grainger, B. Gilbert, Dispersal and diversity in experimental metacommunities: Linking theory and practice. *Oikos* **125**, 1213–1223 (2016).
75. P. Amarasekare, R. M. Nisbet, Spatial heterogeneity, source-sink dynamics, and the local coexistence of competing species. *Am. Nat.* **158**, 572–584 (2001).
76. M. Loreau, N. Mouquet, A. Gonzalez, Biodiversity as spatial insurance in heterogeneous landscapes. *Proc. Natl. Acad. Sci. U.S.A.* **100**, 12765–12770 (2003).
77. N. Mouquet, M. Loreau, Community patterns in source-sink metacommunities. *Am. Nat.* **162**, 544–557 (2003).
78. R. U. Edgehill, R. K. Finn, Activated sludge treatment of synthetic wastewater containing pentachlorophenol. *Biotechnol. Bioeng.* **25**, 2165–2176 (1983).
79. R. W. Babcock, K. S. Ro, C. C. Hsieh, M. K. Stenstrom, Development of an off-Line enricher-reactor process for activated-sludge degradation of hazardous wastes. *Water Environ. Res.* **64**, 782–791 (1992).
80. R. Mei, W. T. Liu, Quantifying the contribution of microbial immigration in engineered water systems. *Microbiome* **7**, 144 (2019).
81. R. Mei, J. Kim, F. P. Wilson, B. T. W. Bocher, W. T. Liu, Coupling growth kinetics modeling with machine learning reveals microbial immigration impacts and identifies key environmental parameters in a biological wastewater treatment process. *Microbiome* **7**, 65 (2019).
82. R. Ryser, M. R. Hirt, J. Häussler, D. Gravel, U. Brose, Landscape heterogeneity buffers biodiversity of simulated meta-food-webs under global change through rescue and drainage effects. *Nat. Commun.* **12**, 4716 (2021).
83. N. Cichocki *et al.*, Bacterial mock communities as standards for reproducible cytometric microbiome analysis. *Nat. Protoc.* **15**, 2788–2812 (2020).
84. S. Takahashi, J. Tomita, K. Nishioka, T. Hisada, M. Nishijima, Development of a prokaryotic universal primer for simultaneous analysis of Bacteria and Archaea using next-generation sequencing. *PLoS One* **9**, e105592 (2014).
85. D. P. R. Herlemann *et al.*, Transitions in bacterial communities along the 2000 km salinity gradient of the Baltic Sea. *ISME J.* **5**, 1571–1579 (2011).
86. J. Oksanen *et al.*, Community ecology package. R package (version 2) (2013).
87. C. Koch, S. Günther, A. F. Desta, T. Hübschmann, S. Müller, Cytometric fingerprinting for analyzing microbial intracommunity structure variation and identifying subcommunity function. *Nat. Protoc.* **8**, 190–202 (2013).
88. F. E. Harrell, C. Dupont, Hmisc: Harrell miscellaneous. R package (version 3) (2008).
89. H. Wickham, ggplot2. *Wiley Interdiscip. Rev. Comput. Stat.* **3**, 180–185 (2011).